Supplemental Information

Samples

The details of the petrography, textures, fabrics and mineral chemistry of the Summit Lake and Mt Timothy xenolith suites have been the subject of previous studies (e.g. Ross, 1983; Brearley et al., 1984; Morales et al., 2010; Canil et al., 2021) and for brevity are not repeated at length here. Polished sections of peridotite xenoliths of this study show they are fresh, coarse textured (Harte, 1977), with olivine (1 – 4 mm), orthopyroxene (1 – 4mm), clinopyroxene (0.25 to 1mm) and spinel (< 0.5 mm), typical of other intraplate spinel peridotite xenoliths. Spongy-textured pyroxene forms on some grain boundaries where host lava invasion occurred but these areas are avoided for chemical analysis by analysis of 50 microns from such grain boundaries.

Analytical Methods

For the Mt Timothy xenoliths, major element mineral chemical data for all phases and trace elements (Sc, Ti, V, Ni, Sr, Y, Zr, REE) in coexisting orthopyroxene and clinopyroxene were reported in Canil et al (2021). Major elements for Summit Lake samples of this study were measured in olivine, orthopyroxene, clinopyroxene and spinel by EPMA at the University of Alberta using a Cameca SX100 instrument in wavelength dispersive mode with a fully-focussed, 20 keV and 40 nA point beam, counting for 16 seconds on peak for Na, Mg, Al, Si, K, Ca, Ti, Cr, Mn, Ni, Fe (and V Zn in spinel only). Trace elements (Sc, Ti, V, Ni, Sr, Y, Zr, REE) in coexisting orthopyroxene and clinopyroxene (4-6 different grains per sample) for Summit Lake samples reported here were measured by laser ablation ICP MS at the University of Victoria using a Cetac 213 nm Nd YAG laser with a 100 µm spot size rastered for 200 µm line length at a scan rate of 20 µm/sec. A background signal was measured for 30 secs, prior to a 60 sec ablation using a fluence of 2.7 J cm^{-2} at 5 Hz. The laser ablations were in He carrier gas flowing to an Agilent 8800 QQQ ICP MS operated in single quadrupole mode. The MPI DING glasses (ML-3B, GOR-132 - Jochum et al., 2005) served as standards and analysis of a BCR2-g glass was used as a check on accuracy. Calibration was carried out every 12 unknowns.

In this study, the Ca and Al in olivine of both Summit Lake and Mt Timothy samples (4-6 different grains per sample) was measured using LA ICPMS with the same laser conditions as the pyroxenes, but with a calibration employing natural olivines as internal lab standards. The olivine standards are all forsterite rich (> Fo_{90}) and had Ca and Al previously measured independently by either solution nebulization ICP MS or high precision EPMA (reported in Wan et al, 2008; D'Souza et al 2020). A three-point standard calibration line for Ca and Al (cps vs. concentration) was measured every 10 olivine unknowns.

Olivine Standard	Ca (ppm)	Al (ppm)
PAK (Pakistan)	10 (±7)	4 (±5)
SC (San Carlos)	507 (±46)	99 (±16)
SL (phenocryst)	1211(±60)	390 (±19)

The LA ICPMS sessions for both pyroxenes and olivine used Si as the internal standard and processed time resolved spectra offline in a spreadsheet. Data are presented only for analyses with counts above detection limit (> 3σ backgound).

Mineral chemistry

Previous work has documented much of the major element in mineral chemistry from xenoliths at Mt Timothy and Summit Lake (e.g. Ross, 1983; Brearley et al., 1984; Morales et al., 2010; Canil et al., 2021). In our new data for Summit Lake, major elements are homogeneous with no core and rim zonation recognized except occasionally for spinel. The Cr# (Cr/Cr+Al) of spinel and Fo olivine are correlated, possibly a measure of depletion in the samples. Two samples (SL58, SL63) have olivines more Fe-rich (Fo86-88) than most xenoliths, and with low Cr# in spinel. No relation of Ca or Al in Ol to level of depletion in sample, as represented by Cr# of Spinel.

REE in Pyroxenes

Trace element data for pyroxenes in Mt Timothy xenoliths were presented in Canil et al 2021. New data presented here for Summit Lake xenoliths, similarly show two groups of REE patterns in clinopyroxene - one with LREE depletion and another six samples (SL38, 43, 58, 62, 68, 70) with enriched sinusoidal patterns (high Ce/Sm) and high Sr (Figure S1). There is no correlation of these LREE enriched samples with T, depth, nor difference in T between thermometers due to cooling/heating. If the LREE enriched or high Sr is attributed to metasomatism, this is not coupled to T history nor depth of sampling. Similarly, most REE patterns in orthopyroxene are normal LREE depleted, except the same five samples show LREE enrichment (high Ce/Sm) as their coexisting cpx (38, 43, 58, 62, 68, 70). (Figure S1).

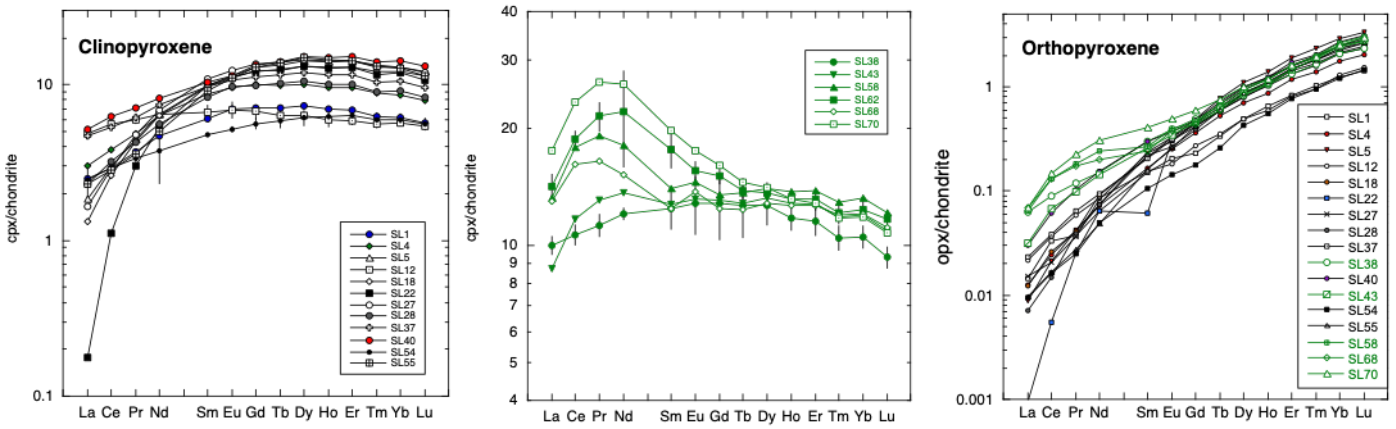

Figure S1 – Rare earth element profiles of clino- and orthopyroxenes.

Ca and Al in Olivine

The Ca and Al contents of olivine are clearly distinct between the Summit Lake and Mt Timothy suites. Summit Lake olivines contain far higher Al (119-215 ppm) and Ca (680-410 ppm) compared to Mt Timothy (42-127 ppm Al, 303 -534 Ca). The variation of Ca and Al in olivine

within individual samples was small, < 10% for Ca and <12% for Al, in both suites. The differing Ca and Al contents on olivine in the two suites cannot be related to the bulk level of the depletion in samples, as this is not markedly different as measured by the Cr# of spinel (0.06 – 0.28 for SL compared to 0.1 - 0.4 for MT) or the Yb abundance of clinopyroxene (Yb_N = 6-15 for SL, 9 – 13 for MT, where 'N' is chondrite-normalized). The Ca and Al contents of olivine are most consistent with lower pressures and/or hotter temperatures for the Summit Lake samples.

Thermobarometry

Geobarometry based on all four phases (olivine, orthopyroxene, clinopyroxene and spinel) in peridotite was possible on 17 and 14 samples, from Mt Timothy and Summit Lake, respectively. Temperature differences between different thermometers are consistent (~ 80 °C) and follow the same patterns of T_{REE} > T_{BKN} > T_{Al} at both Summit Lake and Mt Timothy (Figure S2). The temperatures and patterns show no relationship to LREE enrichment (Ce/Sm), Sr in pyroxenes or any other indicator of metasomatism in the samples, which can be argued to be ancient (Canil et al., 2021).

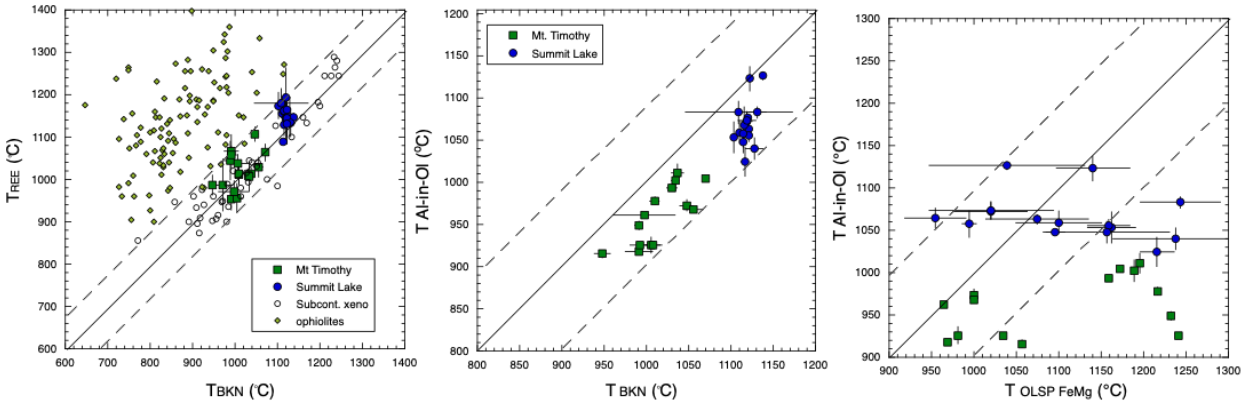

Figure S2 – omparison of geothermometers applied to Summit Lake and Mt. Timothy xenoliths using exchange of Ca-Mg-Fe (T_{BKN}) or REE (T_{REE}) between pyroxene, and exchange of Al (T AL-in-Ol) or Fe-Mg ($T_{OLSP\ FeMg}$) between olivine and spinel. Data are given the in the Data Repository. Data for ophiolite peridotites are compilations from Liang et al (2013) and Canil et al (2021b).

The Ca content of olivine in equilibrium with clinopyroxene is pressure sensitive enough as a barometer (P_{KB}, P_{SC}) but is also significantly T sensitive (~ 60 °C/GPa - Kohler and Brey, 1990; Shejwalkar and Coogan, 2013). The T dependence of P_{KB} greatly affects absolute estimates of depth. A recent study showed, however, that Al exchange with spinel is a thermometer (T_{Al}) that is independent of pressure to 3 GPa (D'Souza et al., 2020). In samples containing olivine, orthopyroxene, clinopyroxene and spinel we can combine two different thermometers T_{Al} and T_{BKN} with two barometers P_{KB} or P_{SC} to derive the pressure (depth) of sampling of the host lava. When applied to the xenoliths of this study, the T_{Al}-P_{KB} combination gives geologically reasonable depths of sampling at Mt Timothy (40 – 85 km), but 10 – 50 km depths in the SL, with many samples far above the Moho in the crust (Figure S3). The results improve somewhat

(15-50 km) using a T_{Al}-P_{SC} which accounts for changing olivine Mg/Fe (T_{Al}- P_{SC}). Conversely, using T_{BKN} produces a depth of sampling of 30 – 55 km at SL, consistent with a Moho near 33 km but depths of 70 – 100 km at Mt Timothy. The latter values are suspect given they are mostly beyond the expected stability of fertile spinel peridotite commonly sampled as xenoliths of the Cordillera, which is stable to 70 – 75 km maximum, before transformation to garnet peridotite (Canil et al., 2021a). Irrespective of thermometer-barometer combinations, the P(depth) for a given combination is always greater for samples from Mt Timothy, compared to Summit Lake (Figure S3).

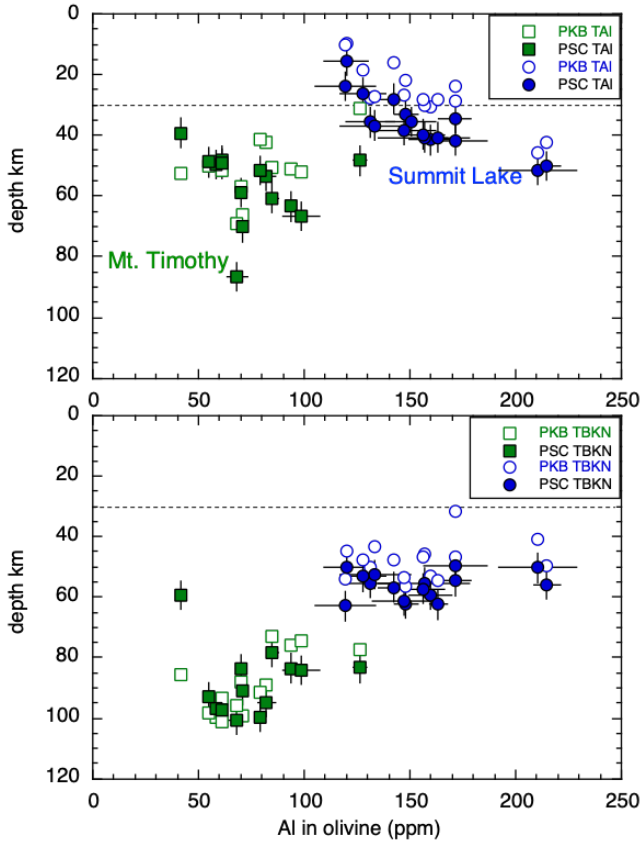

Figure S3 – Comparison of results for various thermometer - barometer combinations applied to the Summit Lake and Mt. Timothy xenoliths.

The depletion history in samples measured by the proxy of Cr# spinel or Fo in olivine also show no correlations to depth or T. The differences in temperature recorded by various geothermometers shown in Figure S2 follows the different closure temperatures or cation exchange in each thermometer at a given cooling rate (Figure S4), calculated after the method of Dodson (1973) assuming various cooling rates for common grain sizes for minerals in peridotite xenoliths and using the following sources for diffusion data: REE in orthopyroxene (Cherniak and Liang (2007), Fe–Mg in clinopyroxenes (Dimonov and Wiedenbeck, 2006), Ca in olivine (Coogan et al, 2005) Al in olivine (Zhukova et al. , 2017).

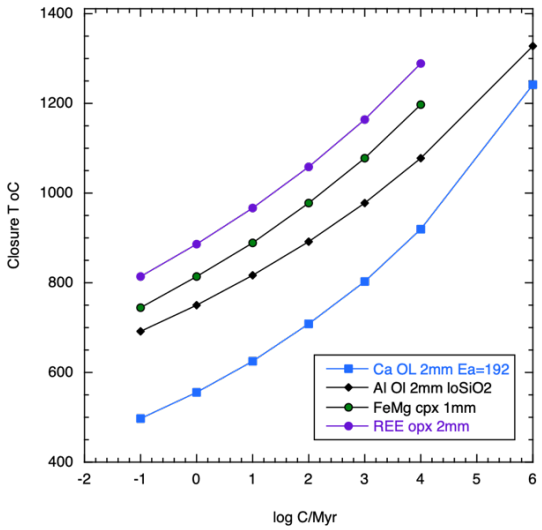

Figure S4 - Closure temperatures calculated for each cation exchange thermometer at a given cooling rate from the Dodson equation.

Geotherm Modelling

We create a model geotherm for the crustal and mantle lithosphere that honours geophysical and petrological datasets. We constrain the model geotherms for lithosphere underlying the Mount Timothy and Summit Lake volcanic centres using the new geothermobarometry data derived from peridotite xenoliths. The model steady-state geotherm for the lithosphere assumes conductive heat flow in a two layer (crust and mantle) lithosphere (cf. Greenfield et al. 2013) comprising: i) a crust of specified thickness (Z_M) having a constant surface temperature (T_0) and surface heat flow (q_0), and ii) a mantle of unspecified thickness (Fig. S5).

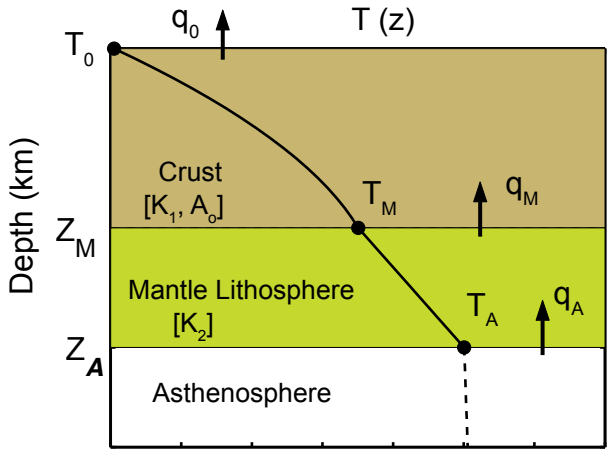

Figure S5. Schematic representation of model for conductive heat transfer in the crust and mantle lithosphere. Variables include: temperature and heat flow at the Earth's surface (T_0, q_0), at the Moho (T_M, q_M), and at the top of the asthenosphere (T_A, q_A), thermal conductivity and heat production in the crust (K_1, Ao) and mantle lithosphere (K_2), and the depths to the Moho (Z_M) and the top of the asthenosphere (Z_A).

The two layers share the same, but unknown, temperature (T_M) at their interface taken as the Moho. Crustal heat production (A(z) is modelled as a function of depth as Ao $e^{(-z/D)}$ where Ao is the heat production at surface and D is taken as the depth to the Moho where heat production falls to ~ 1/3 of the value of Ao. Heat production in the mantle lithosphere is assumed negligible. The physical properties ascribed to the model layers of crust and mantle are listed in Table S4.

Table S4. Physical parameters used in modelling of geotherm (see text).

Property	Layer 1 Crustal Lithosphere	Layer 2 Mantle Lithosphere
T_0 [°C]	10	-
Z_M [km]	25 or 33	
Ao [μW m^{-3}][a]	1.3 ±0.3	0
K [W m^{-1} K^{-1}]	2.5	3.2
ρ [kg m^{-3}]	2800	3300
T_x [°C] (SL)		1126
Z_x [km] (SL)		51 ±5
T_x [°C] (MT)		982
Z_x [km] (MT)		66 ±5

[a]Optimal values used by Greenfield et al. (2013) and adopted from Lewis et al. (1992).

The steady-state conductive temperature distribution for our model one-dimensional (z) crustal lithosphere discussed above is given by:

$$T(z) = T_0 + \frac{q_0\, z}{K_1} + \frac{Ao\, Z_M^2}{K_1}\left(1 - \frac{z}{Z_M} - e^{-z/Z_M}\right) \qquad 0 < z < Z_M \ . \quad (1)$$

The values of q_0 are coupled to the form of the heat production equation and dictated by the relationship:

$$q_0 = 0.3679\, Z_M\, Ao + \frac{(T_M - T_0)\, K_1}{Z_M} \qquad (2)$$

and, therefore, also dependent on the depth and temperature of the Moho. The lithospheric mantle is coupled to the crust by the Moho temperature (T_M) and the reduced heat flow (q_M). The expected steady-state temperature distribution in the mantle lithosphere is described by:

$$T(z) = T_M + \frac{[q_0 - 0.6321\, Ao\, Z_M]}{K_2}\,(z - Z_M) \qquad Z_M < z < Z_a \ . \qquad (3)$$

Our approach takes advantage of the fact that we have geobarometry results that estimate both T and P for each xenolith of peridotite. In each case (i.e. Summit lake and Mount Timothy) we force the model crustal-mantle geotherm through the deepest and hottest xenolith *(T_x-Z_x)*; that single coordinate pair is suffice to define the geotherm (i.e. Eqs. 1-3). Setting Eq. 1 to the depth of the Moho yields:

$$T_M = T_0 + \frac{q_0\, Z_M}{K_1} + 0.3679\, \frac{Ao\, Z_M^2}{K_1} . \quad (4)$$

Inserting the coordinate pair T_x-Z_x into Eq. 3 and rearranging defines T_M:

$$T_M = T_x - \frac{[q_0 - 0.6321\ Ao\ Z_M]}{K_2}\ (Z_x - Z_M) \quad . \qquad (5)$$

Subtracting Eq. 4 from Eq 5 and rearranging yields a functional relationship between Ao and q0 such that choosing values of Ao dictates q0 and the crustal-mantle geotherm is defined:

$$q_0 = \frac{a}{c}\ Ao + \frac{b}{c} \qquad (5)$$

Where:

$$a = \frac{[0.3679\ Z_M^2]}{K_1} + \frac{[0.6321\ Z_M\ (Z_x - Z_M)]}{K_2} \quad , \quad (6a)$$

$$b = \frac{Z_M}{K_1} + \frac{(Z_x - Z_M)}{K_2} \quad , \quad (6b)$$

and

$$c = T_x - \frac{[q_0 - 0.6321\ Ao\ Z_M]}{K_2}\ (Z_x - Z_M) \quad . \quad (6c)$$

Geobarometric estimates of pressure (kb) for the deepest xenoliths were converted to depth (m) as (Table S1):

$$Z_x = \frac{P_x\ 10^8 - 9.8\ \rho_c\ Z_M}{9.8\ \rho_m} + Z_M \quad . \quad (7)$$

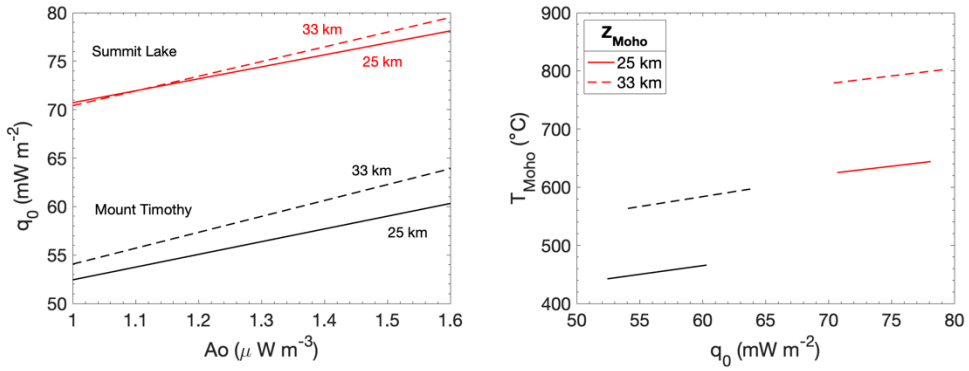

Figure S6: Model co-dependence of parameters on values of *Ao*. (A) Values of q_0 dictated by preferred values of *Ao* (Table S1) for crustal thicknesses of 25 and 33 km and the deep mantle temperatures (T_x) underlying Summit Lake and Mount Timothy. Higher values of T_x dictate higher values of q_0. Thicker crust also supports higher surface heat flow. (B) Model values of Moho temperature (T_M) for Summit lake and Mount Timothy settings (i.e. T_x, Z_x) and for different values of Z_M. Moho temperatures are ~200 °C higher for Summit Lake and thicker crust suggests an increase of 100-150 °C in T_M.

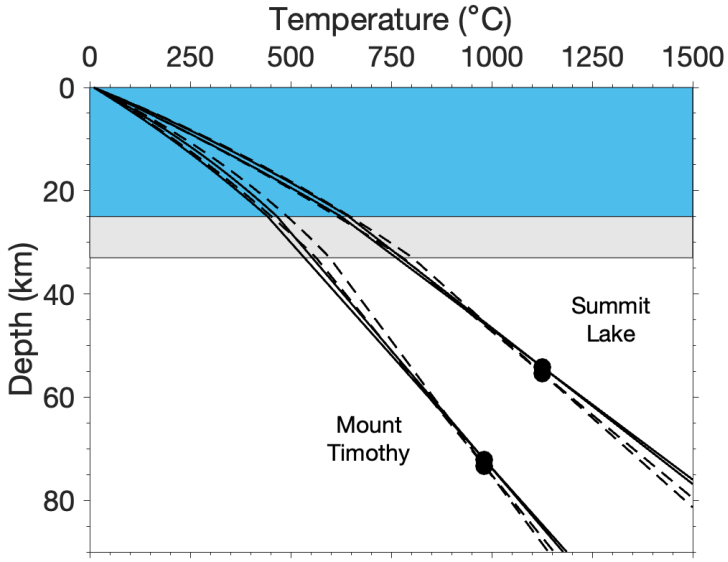

Figure S7. Model geotherms for lithosphere underlying Summit Lake and Mount Timothy constrained to intersect the temperature of the deepest xenoliths (solid dots) for T_M values of 25 km (solid lines) and 33 km (dashed lines) and a range of values for *Ao* (1.0 – 1.6 μW m^{-3}). See Table S5 for output parameters.

Table S5. Output from geotherm models for Summit Lake and Mount Timothy based on a range of *Ao* values (1.3 ±0.3 μW m^{-3}).

Z_M [km]	SL	MT
T_x [°C]	1126	982
P_x [kb]	16.3	22.1
Z_x [km]	54 - 55 (±5)	72 – 73 (±5)
q_0 [mW m^{-2}]	70.4 – 79.5	52.4 – 63.9
T_M [°C] 25 km	625 - 644	442 - 466
T_M [°C] 33 km	779 - 803	563 - 597

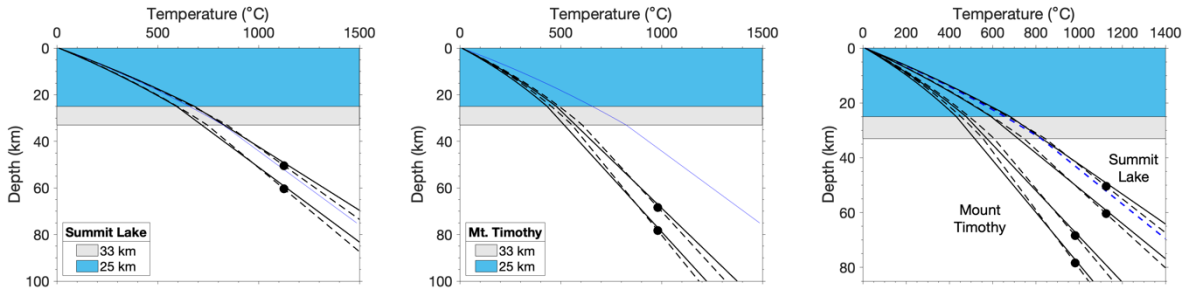

Figure S5. Model geotherms for lithosphere underlying Summit Lake and Mount Timothy constrained to intersect the temperature of the deepest xenoliths (solid dots) and allowing for +/-5 km uncertainty in depth. Blue line is geotherm for Rayfield River from Greenfield et al. (2013).

References

Brearley, M., Scarfe, C., Fujii, T., 1984, The petrology of ultramafic xenoliths from Summit Lake, near Prince George, British Columbia. Contributions to Mineralogy and Petrology, v. 88, p. 53-63.

Canil, D., Russell, J.K., Fode, D. 2021, A test of models for lithosphere foundering or replacement in the Canadian Cordillera using peridotite xenolith geothermometry. Lithos, doi.org/10.1016/j.lithos.2021.106329

Cherniak D.J., Liang Y., 2007, Rare earth element diffusion in natural enstatite. Geochimica et Cosmochimica Acta v. 71, p. 1324–1340. https ://doi. org/10.1016/j.gca.2006.12.001

Coogan , L.A., Hain, A., Stahl, S., Chakraborty, S. 2005, Experimental determination of the diffusion coefficient for calcium in olivine between 900°C and 1500°C, Geochimica et Cosmochimica Acta, v.69, p.3683–3694.

Dimonov A., Weidenbeck M., 2006, (Fe,Mn)–Mg interdiffusion in natural diopside: effect of pO2. European Journal of Mineralogy v. 18,p. 705–718.

Dodson M.H., 1973, Closure temperature in cooling geochronological and petrological systems. Contributions to Mineralogy and Petrology v. 40, p. 259–274. https ://doi.org/10.1007/BF003 7379

Greenfield, A.M.R., Ghent, E.D., Russell, J.K., 2013, Geothermobarometry of spinel peridotites from southern British Columbia: implications for the thermal conditions in the upper mantle. Canadian Journal of Earth Sciences, v. 50, p. 1019–1032.

Kohler, T.P., Brey, G.P., 1990, Calcium exchange between olivine and clinopyroxene calibrated aa geotherombarometer for natural peridotites from 2 to 60 kb with applications. Geochim Cosmochim Acta, v. 54, p. 2375-2388.

Lewis, T.J., Bentkowski, W., Hyndman, R.D., 1992, Crustal temperatures near the Lithoprobe southern Canadian cordillera transect. Canadian Journal of Earth Sciences, v. 29, p. 1197-1214.

Liang, Y., Sun, C., Yao, L., 2013, A REE-in-two-pyroxene thermometer for mafic and ultramafic rocks. Geochimica et Cosmochimica Acta. doi:10.1016/j.gca.2012.10.035

Morales, L.F.G., Tommasi, A., 2011, Composition, textures, seismic and thermal anisotropies of xenoliths from a thin and hot lithospheric mantle (Summit Lake, southern Canadian Cordillera), Tectonophysics, v. 507, p. 1–15

Ross, J.V., 1983, The nature and rheology of the Cordilleran upper mantle of British Columbia: Inferences from peridotite xenoliths. Tectonophysics, v. 100, p. 321-357.

Shejwalkar, A., Coogan, L.A., 2013, Experimental calibration of the roles of temperature and composition in the Ca-in-olivine geothermometer at 0.1 MPa, Lithos, v. 177, p. 54-60.

Zhukova, E., O'Neilll, H.St.C, Campbell, I.H. , 2017, A subsidiary fast-diffusing substitution mechanism of Al in forsterite investigated using diffusion experiments under controlled thermodynamic conditions. Contributions to Mineralogy and Petrology, v. 172, p. 53-66.